JCTC Journal of Chemical Theory and Computation

Excited States in Solution through Polarizable Embedding

Jógvan Magnus Olsen,[†] Kęstutis Aidas,[‡] and Jacob Kongsted*,[†]

Department of Physics and Chemistry, University of Southern Denmark, Campusvej 55, DK-5230 Odense M, Denmark, and Department of Chemistry, H. C. Ørsted Institute, University of Copenhagen, Universitetsparken 5, DK-2100 Copenhagen Ø, Denmark

Received July 8, 2010

Abstract: We present theory and implementation of an advanced quantum mechanics/molecular mechanics (QM/MM) approach using a fully self-consistent polarizable embedding (PE) scheme. It is a polarizable layered model designed for effective yet accurate inclusion of an anisotropic medium in a quantum mechanical calculation. The polarizable embedding potential is described by an atomistic representation including terms up to localized octupoles and anisotropic polarizabilities. It is generally applicable to any quantum chemical description but is here implemented for the case of Kohn−Sham density functional theory which we denote the PE-DFT method. It has been implemented in combination with time-dependent quantum mechanical linear and nonlinear response techniques, thus allowing for assessment of electronic excitation processes and dynamic ground- and excited-state molecular properties using a nonequilibrium formulation of the environmental response. In our formulation of polarizable embedding we explicitly take into account the full self-consistent many-body environmental response from both ground and excited states. The PE-DFT method can be applied to any molecular system, e.g., proteins, nanoparticles and solute−solvent systems. Here, we present numerical examples of solvent shifts and excited-state properties related to a set of organic molecules in aqueous solution.

1. Introduction

Accurate modeling of excited states and molecular properties of large molecular samples represents one of the greatest challenges to modern quantum chemistry. The description of excited states requires the use of quantum mechanics. However, in many cases it is not necessary to use a full quantum mechanical description of the total system. This is, for example, the case when dealing with a solute−solvent system or in more general terms a molecule subjected to a structured environment. In these cases the part of the system not directly involved in the electronic processes can be described effectively using, e.g., classical mechanics. Even though linear scaling techniques are becoming more advanced and may be used to describe larger and more complex systems,[1] effects due to conformational sampling still persist and may become more important as the size of the molecular system is increased. In fact, in many cases it is mandatory to include effects of nuclear dynamics in combination with the electronic structure in order to pursue a direct comparison with experimental data. Thereby, formulation of accurate effective Hamiltonian methods becomes of crucial importance. This should particularly be seen in the light of recent trends aiming at a complete quantitative description of biological functions with the necessary step of bringing quantum chemistry into the life sciences.[2]

With the aim of describing large molecular systems we present in this paper a focused model based on the quantum mechanics/molecular mechanics (QM/MM) approach using a fully self-consistent polarizable embedding scheme which we denote the polarizable embedding (PE) model. The electrostatic embedding potential, i.e., the permanent charge distribution of the environment, is represented by a multi-

* Corresponding author e-mail: kongsted@ifk.sdu.dk.
[†] University of Southern Denmark.
[‡] University of Copenhagen.

10.1021/ct1003803
Published on Web 10/26/2010

center multipole expansion. The expansion centers are defined to be located either at the atomic nuclei of the molecules defining the environment or at the atomic nuclei and bond midpoints. The latter description would, in principle, lead to a more accurate representation of the embedding potential with an improved radius of convergence for the multipole model. The electrostatic embedding potential only accounts for the permanent charge distribution of the environment, and in order to account for many-body induction effects, i.e., the polarization of the environment both internally and by the quantum mechanical core, we assign a set of localized anisotropic dipole polarizability tensors at the expansion centers, giving rise to an induced charge distribution in the environment. The latter is represented in terms of induced dipoles which are determined on the basis of classical response theoretical methods.[3] The localized multipoles and polarizabilities are determined using quantum mechanical methods. In this paper we show that a careful representation of the permanent and induced potentials by multipoles and polarizabilities, respectively, leads to a very accurate mid- and long-range electrostatic potential as compared to quantum mechanical data. The PE model is generally applicable but here it is implemented for the case of Hartree−Fock and Kohn−Sham density functional theory, which we denote the PE-HF and PE-DFT methods. The functional form of the polarizable embedding potential resembles that of the EFP method by Gordon et al.;[4−6] however, the strength of our model is the ability to describe excited states on the same footing as ground states. This is achieved through a formulation of the PE model within the context of time-dependent quantum mechanical response theory. Pertinent to our formulation of polarizable embedding within response theory is the self-consistent many-body environmental response. Here it is important to emphasize that the response of the environment due to the differential change between the ground- and excited-state electron density is fully self-consistent, whereas this is approximated in other similar implementations.[7−10] The consequences of typical approximations as compared to the inclusion of the fully self-consistent environmental response is investigated with numerical examples. The PE model is presented and implemented up to and including quadratic response, with the possibility of straightforwardly extending it to higher order response. This allows for evaluation of vertical electronic excitation energies and the related one- and two-photon transition moments. Furthermore, electronic second- and third-order ground-state molecular properties, such as static and dynamic (hyper)polarizabilities, are available, as are excited-state first-order molecular properties. In addition, magnetic properties, such as magnetizabilities, nuclear shielding constants, and spin−spin coupling constants, may also be computed, using gauge invariant atomic orbitals (GIAOs) when needed.

Nuclear dynamics is in the present method considered by performing classical molecular dynamics (MD) simulations. Here we proceed in a sequential manner; i.e., we first perform the MD simulations and then, using an appropriate number of configurations extracted from the MD simulations, simulate the electronic structure. In this respect we neglect the effect of the electronic structure on the configurations, and the accuracy of our approach relies first of all on the use of an accurate classical potential to be used for the MD simulations.

Inclusion of explicit polarization into force field methods have in recent years received much attention.[11] The current status is that polarization may contribute significantly and specifically to specific solvation process. For example, polarization causes a significant increase in the dipole moment of a water molecule in the liquid state and may in addition constitute as much as 50% of the total interaction energy.[12] An important point here is to be able to calculate all properties characterizing the intermolecular interactions by quantum mechanical methods.

In the present paper the focus is on the effects from a water solvent on the excitation energies of a set of organic molecules, i.e., the solvent shifts. We emphasize that our computational method is not restricted to consideration of solute−solvent systems. However, predictions and rationalizations related to solvent shifts have, for a long time, been a very active and important research area in chemistry[13−17] and serve here as a valuable benchmark for this newly developed computational method. Furthermore, solvent shifts are also highly relevant to, e.g., the studies of biological samples. In fact, certain organic molecules are frequently used as molecular chameleons in order to characterize the degree of polarity of an environment. This is possible since a change in the environmental polarity will lead to a differential stabilization of the ground and excited states of the probe molecule, and thereby to a change in the energy difference between these two states. Consequently, variations in the intensity and especially the position of the absorption or emission spectra becomes a direct measure of the polarity and related specific interactions between the probe and the environment. The key to an accurate rationalization and modeling of, e.g., such chameleons is a flexible computational model formulated toward excited states of large molecular samples.

2. Theory

Below we detail the theoretical aspects of the PE model and its formulation within Kohn−Sham density functional theory and time-dependent response theory.

2.1. Ground-State Polarizable Embedding. The PE model presented in this work uses the QM/MM approach[18−22] to describe the interactions between the environment and the central molecular system. We use an advanced force field representation of the environment which is derived by quantum mechanical calculations. Thus, we assign a multicenter multipole expansion to each molecule in the surrounding environment to represent the electrostatic embedding potential. Furthermore, we place localized anisotropic dipole−dipole polarizability tensors on all expansion centers to allow polarization of the electrostatic embedding potential. This enables us to formulate the PE model where the ground-state electron density of the molecular core is optimized while simultaneously taking into account the explicit electrostatic interactions and many-body induction effects of the surrounding environment in a self-consistent manner. All other

interactions, mainly short-range repulsion and dispersion, can be modeled with a standard 6−12 Lennard-Jones (LJ) potential. The LJ potential does not depend on electronic coordinates and will therefore not affect the electron density of the molecular core.

We begin by describing the general PE model and will later apply it to density functional theory (DFT). Our model focuses on a central molecular system which we will refer to as the QM core. The effects from interactions with the environment are described through the PE potential. The energy of the QM core can thus be separated into two terms

$$E_{\text{PE-QM}} = E_{\text{QM}} + E_{\text{PE}} \tag{1}$$

where E_{QM} is the energy of the isolated QM core and E_{PE} is the energy due to the interactions with the PE potential. The interaction energy, E_{PE}, is given by

$$E_{\text{PE}} = E_{\text{PE}}^{\text{es}} + E_{\text{PE}}^{\text{ind}} + E_{\text{PE}}^{\text{LJ}} \tag{2}$$

where $E_{\text{PE}}^{\text{es}}$ is the electrostatic interaction energy, $E_{\text{PE}}^{\text{ind}}$ is the induction energy, and $E_{\text{PE}}^{\text{LJ}}$ is the energy due to the LJ interactions. The electrostatic contribution is composed of interactions between the permanent multipoles in the environment and the nuclei and electrons in the QM core; i.e.,

$$E_{\text{PE}}^{\text{es}} = \sum_{s=1}^{S}\sum_{k=0}^{K}\frac{(-1)^k}{k!}\left(\sum_{m=1}^{M} Z_m \mathbf{T}_{ms}^{(k)} - \sum_{i=1}^{N}\mathbf{T}_{is}^{(k)}\right)\mathbf{Q}_s^{(k)} \tag{3}$$

Here S is the total number of sites in the environment and K is the maximum order of the multipole expansion assigned to the molecules in the environment. The quantities M and N are the numbers of nuclei and electrons, respectively, in the QM core. The $\mathbf{T}^{(k)}$ factors are the interaction tensors, defined as $\mathbf{T}_{ab}^{(k)} = \nabla^k[1/(|\mathbf{r}_b - \mathbf{r}_a|)]$, and $\mathbf{Q}_s^{(k)}$ is the kth order multipole moment assigned to the sth site in the environment; e.g., $\mathbf{Q}_s^{(0)} = q_s$, $\mathbf{Q}_s^{(1)} = \boldsymbol{\mu}_s$, and so on.

The induction energy due to the polarization of the environment both internally and by the QM core is given by

$$E_{\text{PE}}^{\text{ind}} = -\frac{1}{2}\boldsymbol{\mu}^{\text{ind}} \cdot (\mathbf{F}^{\text{nuc}} + \mathbf{F}^{\text{elec}} + \mathbf{F}^{\text{es}}) \tag{4}$$

where $\boldsymbol{\mu}^{\text{ind}}$ is a $3S$-dimensional vector which contains the full set of induced dipole moments, i.e., $\boldsymbol{\mu}^{\text{ind}} = [\boldsymbol{\mu}_1^{\text{ind}}, \boldsymbol{\mu}_2^{\text{ind}}, ..., \boldsymbol{\mu}_S^{\text{ind}}]^{\text{T}}$, and $\mathbf{F}^{\text{nuc}}$, $\mathbf{F}^{\text{elec}}$, and $\mathbf{F}^{\text{es}}$ are the corresponding electric field vectors, which contain the electric fields from the nuclei and electrons in the QM core and the permanent multipole moments in the environment at the positions of the induced dipoles. An induced dipole moment is determined by the total electric field which is the sum of the fields from the nuclei and electrons in the QM core and the permanent multipoles and all the other induced dipoles in the environment. The set of induced dipoles can be conveniently determined as a simple matrix−vector multiplication[3]

$$\boldsymbol{\mu}^{\text{ind}} = \mathbf{B}(\mathbf{F}^{\text{nuc}} + \mathbf{F}^{\text{elec}} + \mathbf{F}^{\text{es}}) = \mathbf{BF} \tag{5}$$

where $\mathbf{B}$ is the symmetric $(3S \times 3S)$-dimensional classical response matrix connecting the electric fields and the set of induced dipoles. The response matrix is defined as

$$\mathbf{B} = \begin{pmatrix} \boldsymbol{\alpha}_1^{-1} & \mathbf{T}_{12}^{(2)} & \cdots & \mathbf{T}_{1S}^{(2)} \\ \mathbf{T}_{21}^{(2)} & \boldsymbol{\alpha}_2^{-1} & \ddots & \vdots \\ \vdots & \ddots & \ddots & \mathbf{T}_{(S-1)S}^{(2)} \\ \mathbf{T}_{S1}^{(2)} & \cdots & \mathbf{T}_{S(S-1)}^{(2)} & \boldsymbol{\alpha}_S^{-1} \end{pmatrix}^{-1} \tag{6}$$

where the polarizability tensors are along the diagonal and the off-diagonal elements are the dipole−dipole interaction tensors.

The PE model is applied to DFT by constructing an effective Kohn−Sham (KS) operator; i.e.,

$$\hat{f}_{\text{eff}} = \hat{f}_{\text{KS}} + \hat{v}_{\text{PE}} \tag{7}$$

where $\hat{f}_{\text{KS}}$ is the ordinary vacuum Kohn−Sham operator and $\hat{v}_{\text{PE}}$ is the PE potential operator. The contribution to the effective KS operator due to the polarizable environment, i.e., the PE potential operator $\hat{v}_{\text{PE}}$, is determined by minimization of the total energy functional with respect to the electron density. Therefore, we only need to consider terms that depend on the electron density, i.e., the last term in eq 3, where the electron charge is replaced by an integral over the density, and eq 4 which has a density dependence through the electric field from the electrons both explicitly and through the induced dipole moments (eq 5). Thus, the PE contribution in second quantized (SQ) form is found to be

$$\hat{v}_{\text{PE}} = \sum_{s=1}^{S}\sum_{k=0}^{K}\frac{(-1)^{(k+1)}}{k!}\mathbf{Q}_s^{(k)}\sum_{pq}\mathbf{T}_{s,pq}^{(k)}\hat{E}_{pq} - \sum_{s=1}^{S}\boldsymbol{\mu}_s^{\text{ind}}(\mathbf{F}[\rho])\sum_{pq}\mathbf{T}_{s,pq}^{(1)}\hat{E}_{pq} \tag{8}$$

where the subscripts pq indicate a matrix element of the corresponding operator in the KS orbital basis. The excitation operator $\hat{E}_{pq}$ is expressed in terms of creation and annihilation operators, i.e., $\hat{E}_{pq} = a_{p\alpha}^{\dagger}a_{q\alpha} + a_{p\beta}^{\dagger}a_{q\beta}$. The first term in eq 8 contains the electrostatic embedding potential introduced here in terms of a set of localized multipole moments, while the second term accounts for polarization of the environment by the electron density. The induced dipole moments are updated in each self-consistent field (SCF) iteration, thus leading to a fully self-consistent treatment of the polarization. The derivation of the PE-HF method proceeds in a similar manner with the construction of an effective Fock operator.

2.2. Polarizable Embedding for Excited States. In this work we will only give an overview of the derivation of the linear and quadratic quantum mechanical response functions with emphasis on the contributions that are due to the PE potential. For a detailed discussion of the implementation of linear and quadratic response theory in vacuum, we refer the reader to the work by Sałek et al.[23]

The starting point for the derivation of the response functions is to consider the time dependence of an expectation value of a time-independent operator $\hat{A}$. It can be expanded in orders of a time-dependent perturbation

$$\langle t|\hat{A}|t\rangle = \langle t|\hat{A}|t\rangle^{(0)} + \langle t|\hat{A}|t\rangle^{(1)} + \langle t|\hat{A}|t\rangle^{(2)} + ... \tag{9}$$

where the first term on the right-hand side is the time-independent expectation value and the second and third terms

describe the linear and quadratic response to the perturbation, respectively. The Fourier representation of the linear and quadratic response is given by

$$\langle t|\hat{A}|t\rangle^{(1)} = \int \langle\langle \hat{A};\hat{V}^{\omega}\rangle\rangle_{\omega} \exp(-i\omega t)\, d\omega \tag{10}$$

$$\langle t|\hat{A}|t\rangle^{(2)} = \frac{1}{2}\int\int \langle\langle \hat{A};\hat{V}^{\omega_1},\hat{V}^{\omega_2}\rangle\rangle_{\omega_1,\omega_2} \exp(-i(\omega_1 + \omega_2)t)\, d\omega_1\, d\omega_2 \tag{11}$$

where $\langle\langle \hat{A};\hat{V}^{\omega}\rangle\rangle_{\omega}$ and $\langle\langle \hat{A};\hat{V}^{\omega_1},\hat{V}^{\omega_2}\rangle\rangle_{\omega_1,\omega_2}$ are the linear and quadratic response functions, respectively, and $\hat{V}^{\omega}$ is a Fourier transformed perturbation operator; i.e., $\hat{V}(t) = \int \hat{V}^{\omega} \exp(-i\omega t)\, d\omega$. We use an exponential parametrization of the time evolution of the reference Kohn−Sham determinant; i.e., $|t\rangle = \exp(-\hat{\kappa}(t))|0\rangle$, where $|0\rangle$ is the unperturbed Kohn−Sham determinant and $\hat{\kappa}(t)$ is the anti-Hermitian one-electron operator defined as $\hat{\kappa}(t) = \sum_{rs} \kappa_{rs}(t)\hat{E}_{rs}$.

The response functions are derived using the Ehrenfest theorem, which can be written as[24]

$$\langle 0|[\hat{Q}, \exp(\hat{\kappa}(t))\left(\hat{H}(t) + \hat{V}(t) - i\frac{d}{dt}\right)\exp(-\hat{\kappa}(t))]|0\rangle = 0 \tag{12}$$

where $\hat{Q}$ is a general one-electron time-independent operator which we will define as the vector $\hat{\mathbf{q}}$ containing the excitation operators $\hat{E}_{pq}$. Equation 12 is then expanded in a Baker−Campbell−Hausdorff (BCH) expansion, and perturbation expansions of the time evolution operator $\hat{\kappa}(t)$ and the KS Hamiltonian $\hat{H}(t)$ are inserted. Terms that are first and second order in the perturbation are collected and used to derive the linear and quadratic response functions, respectively, in the frequency domain. The SQ form of the expanded time-dependent Kohn−Sham Hamiltonian is

$$\hat{H}(t) = \sum_n \hat{H}^{(n)} = \sum_n \sum_{pq} f_{pq}^{(n)}\hat{E}_{pq} = \sum_n \sum_{pq} (\delta_{0n}h_{pq} + j_{pq}^{(n)} + \nu_{xc,pq}^{(n)} + \nu_{PE,pq}^{(n)})\hat{E}_{pq} \tag{13}$$

where h_{pq} is an integral over the kinetic energy and nuclear-attraction operators, $j_{pq}^{(n)}$ is an nth-order Coulomb integral and $\nu_{xc,pq}^{(n)}$ is an nth-order integral over the exchange-correlation potential. Finally, the integral $\nu_{PE,pq}^{(n)}$ is an nth-order integral over the PE potential which gives the contribution from the polarizable environment.

2.2.1. Linear Response. The linear response function $\langle\langle \hat{A};\hat{V}^{\omega}\rangle\rangle_{\omega}$ for the property $\hat{A}$ perturbed by a periodic perturbation $\hat{V}^{\omega}$ with associated frequency ω is given by

$$\langle\langle \hat{A};\hat{V}^{\omega}\rangle\rangle_{\omega} = -\mathbf{A}^{\dagger}\boldsymbol{\kappa}^{\omega} \tag{14}$$

where $\mathbf{A} = \langle 0|[\hat{\mathbf{q}},\hat{A}]|0\rangle$ and the time evolution parameters are collected in the vector $\boldsymbol{\kappa}^{\omega}$. The time evolution parameters are determined from the matrix equation

$$(\mathbf{E} - \omega\mathbf{S})\boldsymbol{\kappa}^{\omega} = \mathbf{V}^{\omega} \tag{15}$$

which is derived from the Ehrenfest theorem in eq 12. Here it has been used that $\hat{\kappa}^{\omega} = \hat{\mathbf{q}}^{\dagger}\boldsymbol{\kappa}^{\omega}$. The $\mathbf{E}$ matrix is defined through

$$\mathbf{E}\boldsymbol{\kappa}^{\omega} = -\langle 0|[\hat{\mathbf{q}}, [\hat{\kappa}^{\omega}, \hat{H}^{0}] + \hat{H}^{\omega}]|0\rangle \tag{16}$$

The generalized overlap matrix is defined as

$$\mathbf{S} = \langle 0|[\hat{\mathbf{q}}, \hat{\mathbf{q}}^{\dagger}]|0\rangle \tag{17}$$

and the perturbation vector is given by

$$\mathbf{V}^{\omega} = \langle 0|[\hat{\mathbf{q}}, \hat{V}^{\omega}]|0\rangle \tag{18}$$

We observe that explicit contributions from the PE potential only enter the linear response function through the $\mathbf{E}$ matrix as

$$\mathbf{E}_{PE}\boldsymbol{\kappa}^{\omega} = -\langle 0|[\hat{\mathbf{q}}, [\hat{\kappa}^{\omega}, \hat{v}_{PE}^{0}] + \hat{v}_{PE}^{\omega}]|0\rangle \tag{19}$$

Using one-index transformed integrals,[25] we define a new set of operators

$$\hat{Q}_1^{\omega} = [\hat{\kappa}^{\omega}, \hat{v}_{PE}^{0}] = \hat{v}_{PE}^{0}(\boldsymbol{\kappa}^{\omega}) \tag{20}$$

$$\hat{Q}_2^{\omega} = \hat{v}_{PE}^{\omega} = -\sum_{s=1}^{S} \boldsymbol{\mu}_s^{ind}(\tilde{\mathbf{F}}^{\omega})\hat{\mathbf{T}}_s^{(1)} \tag{21}$$

where the induced dipole moments are determined from eq 5 and the transformed electric field is evaluated according to

$$\tilde{\mathbf{F}}^{\omega} = \langle 0|[\hat{\kappa}^{\omega}, \hat{\mathbf{T}}_s^{(1)}]|0\rangle = \langle 0|\hat{\mathbf{T}}_s^{(1)}(\boldsymbol{\kappa}^{\omega})|0\rangle \tag{22}$$

Finally, we can express the PE contribution to the linearly transformed $\mathbf{E}$ matrix as

$$\mathbf{E}_{PE}\boldsymbol{\kappa}^{\omega} = -\langle 0|[\hat{\mathbf{q}}, \hat{Q}_1^{\omega} + \hat{Q}_2^{\omega}]|0\rangle \tag{23}$$

The $\hat{Q}_1^{\omega}$ operator gives the zero-order PE contribution to the linear response which corresponds to a static environment; i.e., the environment does not respond to the applied perturbation. The $\hat{Q}_2^{\omega}$ operator, on the other hand, describes the dynamical response of the environment due to the perturbation. It is important to note that this is the fully self-consistent many-body environmental response without approximations as opposed to other similar implementations[7,8] where the dynamical response is approximated by using a block-diagonal classical response matrix (eq 6) in the response calculations. The approximated block-diagonal response matrix includes the polarizability tensors but neglects the off-diagonal interaction tensors, whereas we include the full response matrix. The consequences of the approximation is investigated in section 5.2.

2.2.2. Quadratic Response. The quadratic response function $\langle\langle \hat{A};\hat{V}^{\omega_1},\hat{V}^{\omega_2}\rangle\rangle_{\omega_1,\omega_2}$ for the property $\hat{A}$ perturbed by two periodic perturbations $\hat{V}^{\omega_1}$ and $\hat{V}^{\omega_2}$ with associated frequencies ω_1 and ω_2, respectively, is given by

$$\langle\langle \hat{A};\hat{V}^{\omega_1},\hat{V}^{\omega_2}\rangle\rangle_{\omega_1,\omega_2} = \boldsymbol{\kappa}^{\mathbf{A}^{\dagger}}\mathbf{V}^{\omega_1,\omega_2} + \hat{P}_{12}\langle 0|[\hat{\kappa}^{\omega_1}, [\hat{\kappa}^{\omega_2}, \hat{A}]]|0\rangle \tag{24}$$

where the perturbation vector is given by

$$\mathbf{V}^{\omega_1,\omega_2} = \hat{P}_{12}(\langle 0|[\hat{\mathbf{q}},[\hat{\kappa}^{\omega_1},[\hat{\kappa}^{\omega_2},\hat{H}^0]]]|0\rangle + \omega_2\langle 0|[\hat{\mathbf{q}},[\hat{\kappa}^{\omega_1},\hat{\kappa}^{\omega_2}]]|0\rangle + 2\langle 0|[\hat{\mathbf{q}},[\hat{\kappa}^{\omega_1},\hat{H}^{\omega_2}+\hat{V}^{\omega_2}]]|0\rangle + \langle 0|[\hat{\mathbf{q}},\hat{\bar{H}}^{\omega_1,\omega_2}]|0\rangle) \quad (25)$$

Here $\hat{P}_{12}$ is the idempotent symmetrizer defined through $\hat{P}_{12}A(\omega_1,\omega_2) = (1/2)[A(\omega_1,\omega_2) + A(\omega_2,\omega_1)]$. Furthermore, we have used that the second-order density matrix elements can be separated into components due to either first- or second-order parameters such that the Hamiltonian can be similarly separated; i.e., $\hat{H}^{\omega_1,\omega_2} = \hat{\bar{H}}^{\omega_1,\omega_2} + \hat{\bar{\bar{H}}}^{\omega_1,\omega_2}$. The time evolution parameters are determined by solving three linear response equations

$$\kappa^{\mathbf{A}^\dagger}(\mathbf{E} - (\omega_1+\omega_2)\mathbf{S}) = \mathbf{A}^\dagger \quad (26)$$

$$(\mathbf{E} - \omega_1\mathbf{S})\kappa^{\omega_1} = \mathbf{V}^{\omega_1} \quad (27)$$

$$(\mathbf{E} - \omega_2\mathbf{S})\kappa^{\omega_2} = \mathbf{V}^{\omega_2} \quad (28)$$

The explicit PE contributions to the quadratic response function enter the $\mathbf{E}$ matrix and the $\mathbf{V}^{\omega_1,\omega_2}$ vector. Contributions that appear in the $\mathbf{E}$ matrix are analogous to the linear response case; i.e.,

$$\kappa^{\mathbf{A}^\dagger}\mathbf{E}_{\mathrm{PE}} = -\langle 0|[\hat{\mathbf{q}},\hat{Q}_1^{\omega_1,\omega_2} + \hat{Q}_2^{\omega_1,\omega_2}]|0\rangle \quad (29)$$

where

$$\hat{Q}_1^{\omega_1,\omega_2} = [\hat{\kappa}^{\mathbf{A}^\dagger},\hat{v}_{\mathrm{PE}}^0] = \hat{v}_{\mathrm{PE}}^0(\kappa^{\mathbf{A}^\dagger}) \quad (30)$$

$$\hat{Q}_2^{\omega_1,\omega_2} = \hat{\bar{v}}_{\mathrm{PE}}^{\omega_1,\omega_2} = -\sum_{s=1}^{S}\boldsymbol{\mu}_s^{\mathrm{ind}}(\tilde{\mathbf{F}}^{\omega_1,\omega_2})\hat{\mathbf{T}}_s^{(1)} \quad (31)$$

The induced dipoles are calculated using eq 5 and the transformed electric field is given by

$$\tilde{\mathbf{F}}^{\omega_1,\omega_2} = \langle 0|[\hat{\kappa}^{\mathbf{A}^\dagger},\hat{\mathbf{T}}_s^{(1)}]|0\rangle = \langle 0|\hat{\mathbf{T}}_s^{(1)}(\kappa^{\mathbf{A}^\dagger})|0\rangle \quad (32)$$

Contributions to the perturbation vector are obtained from eq 25; i.e.,

$$\mathbf{V}_{\mathrm{PE}}^{\omega_1,\omega_2} = \hat{P}_{12}(\langle 0|[\hat{\mathbf{q}},[\hat{\kappa}^{\omega_1},[\hat{\kappa}^{\omega_2},\hat{v}_{\mathrm{PE}}^0]]]|0\rangle + 2\langle 0|[\hat{\mathbf{q}},[\hat{\kappa}^{\omega_1},\hat{v}_{\mathrm{PE}}^{\omega_2}]]|0\rangle + \langle 0|[\hat{\mathbf{q}},\hat{\bar{v}}_{\mathrm{PE}}^{\omega_1,\omega_2}]|0\rangle) \quad (33)$$

which we can rewrite to a more convenient form by defining the following set of operators:

$$\hat{Q}_3^{\omega_1,\omega_2} = \hat{P}_{12}[\hat{\kappa}^{\omega_1},[\hat{\kappa}^{\omega_2},\hat{v}_{\mathrm{PE}}^0]] = \hat{P}_{12}\hat{v}_{\mathrm{PE}}^0(\kappa^{\omega_2},\kappa^{\omega_1}) \quad (34)$$

$$\begin{aligned}\hat{Q}_4^{\omega_1,\omega_2} &= 2\hat{P}_{12}[\hat{\kappa}^{\omega_1},\hat{v}_{\mathrm{PE}}^{\omega_2}] \\ &= -2\hat{P}_{12}\sum_{s=1}^{S}\boldsymbol{\mu}_s^{\mathrm{ind}}(\tilde{\mathbf{F}}^{\omega_2})[\hat{\kappa}^{\omega_1},\hat{\mathbf{T}}_s^{(1)}] \\ &= -2\hat{P}_{12}\sum_{s=1}^{S}\boldsymbol{\mu}_s^{\mathrm{ind}}(\tilde{\mathbf{F}}^{\omega_2})\hat{\mathbf{T}}_s^{(1)},(\kappa^{\omega_1})\end{aligned} \quad (35)$$

$$\begin{aligned}\hat{Q}_5^{\omega_1,\omega_2} &= \hat{P}_{12}\hat{\bar{v}}_{\mathrm{PE}}^{\omega_1,\omega_2} \\ &= -\hat{P}_{12}\sum_{s=1}^{S}\boldsymbol{\mu}_s^{\mathrm{ind}}(\tilde{\mathbf{F}}^{\omega_1,\omega_2})\hat{\mathbf{T}}_s^{(1)}\end{aligned} \quad (36)$$

Here the perturbed electric field $\tilde{\mathbf{F}}^{\omega_2}$ is defined in eq 22 and $\tilde{\mathbf{F}}^{\omega_1,\omega_2}$ is defined as

$$\tilde{\mathbf{F}}^{\omega_1,\omega_2} = \langle 0|[\hat{\kappa}^{\omega_1},[\hat{\kappa}^{\omega_2},\hat{\mathbf{T}}_s^{(1)}]]|0\rangle = \hat{\mathbf{T}}_s^{(1)}(\kappa^{\omega_2},\kappa^{\omega_1}) \quad (37)$$

The induced dipole moments are determined from eq 5 as before. Using the newly defined operators, we obtain the PE contribution to the perturbation vector as

$$\mathbf{V}_{\mathrm{PE}}^{\omega_1,\omega_2} = \langle 0|[\hat{\mathbf{q}},\hat{Q}_3^{\omega_1,\omega_2} + \hat{Q}_4^{\omega_1,\omega_2} + \hat{Q}_5^{\omega_1,\omega_2}]|0\rangle \quad (38)$$

Just as in the linear response case there are terms, here it is $\hat{Q}_1^{\omega_1,\omega_2}$ and $\hat{Q}_3^{\omega_1,\omega_2}$, that contain the zero-order PE potential operator which also here give the contributions to the response function that arise from a static environment. All the other contributions, i.e., $\hat{Q}_2^{\omega_1,\omega_2}$, $\hat{Q}_4^{\omega_1,\omega_2}$, and $\hat{Q}_5^{\omega_1,\omega_2}$, account for the dynamical response of the environment due to the periodic perturbations.

3. Implementation

The presented PE-DFT method has been implemented in a developmental version of the Dalton program.[26] The implementation also trivially includes the PE-HF method due to the nature of the DFT implementation in the Dalton program. The electrostatic part is currently able to use permanent multipoles up to and including octupoles. The implementation includes the use of anisotropic dipole−dipole polarizability tensors leading to induced dipole moments which are calculated using either a direct or an iterative approach. In the direct approach, which is the default, we calculate the classical response matrix (eq 6) explicitly and store it on disk. The induced dipoles are subsequently calculated using a simple matrix−vector multiplication. This is the most efficient and fastest method; however, for calculations on very large molecular systems and/or on computers with low memory, where it is not possible to form the response matrix explicitly, the iterative approach becomes useful because of very low memory requirements. The iterative approach per default uses the Jacobi method to calculate the induced dipole moments. To avoid the so-called "polarizability catastrophe", we have added the option to use modified dipole interactions according to the model by Thole.[27,28]

The implementation of the contributions to the linear and quadratic response functions is based on the work by Sałek et al.,[23] who implemented DFT and DFT response functions in the Dalton program. Thus, our approach was to add the relevant contributions due to the PE potential to the existing DFT response code. The contributions we considered are

presented in eqs 23, 29, and 38. However, terms which contain zero-order PE contributions $\hat{v}_{PE}^{0}$, i.e., the $\hat{Q}_1^{\omega}$ operator (eq 20) and the $\hat{Q}_1^{\omega_1,\omega_2}$ and $\hat{Q}_3^{\omega_1,\omega_2}$ operators (eqs 30 and 34), are accounted for via the effective zero-order Hamiltonian. In the case of a nonpolarizable environment these are the only terms that contribute since the other terms account for the induced polarization in the environment due to the applied perturbation. The dynamic response of the environment in the linear response part is accounted for by the $\hat{Q}_2^{\omega}$ operator (eq 21) which is formed by first calculating the transformed electric field according to eq 22 and subsequently updating the induced dipoles via eq 5 using the classical response matrix from eq 6 which has been stored on disk during the ground-state optimization. The $\hat{Q}_4^{\omega_1,\omega_2}$ and $\hat{Q}_5^{\omega_1,\omega_2}$ operators (eqs 35 and 36) in the case of quadratic response are constructed in a similar manner using eqs 32 and 37 for the transformed electric fields.

4. Computational Details

To illustrate the capabilities of the implemented PE-DFT method, we here consider the UV/vis vertical absorption energies of a range of organic compounds in aqueous solution. In particular, we have computed the lowest $n \rightarrow \pi^*$ excitation energy of acetone and acrolein as well as the lowest $\pi \rightarrow \pi^*$ excitation energy of acrolein, pyridine, uracil, coumarin 151, and coumarin 153. To model nuclear dynamical effects, we performed classical MD simulations, using a polarizable force field, of each solute in an aqueous environment in order to extract a number of statistically uncorrelated solute−solvent configurations. These configurations were then subjected to the PE-DFT calculations where the solute is treated using DFT and the solvent molecules are represented by a PE potential. The excitation energy in solution is evaluated as the statistical average over the molecular configurations. The solvent shift of the excitation energy is defined as the difference between the excitation energy in solution and in vacuum.

4.1. Molecular Structures, Force Fields, and MD Simulations. In this work, we used the molecular configurations of acetone, *s-trans*-acrolein, and uracil in aqueous solution derived in our previous studies.[17,29,30] However, the computational procedure to obtain the solute−solvent configurations for the rest of the considered molecular probes follows the same strategy. The solvated geometries of pyridine and coumarin 151 were obtained from geometry optimizations using the B3LYP exchange-correlation functional[31] and the aug-cc-pVTZ basis set[32] along with the integral equation formalism PCM model[33] to account for bulk solvent effects. For coumarin 153 we used the same method but the aug-cc-pVDZ basis[32] due to cost-effectiveness, and we only considered the lowest energy conformation as obtained from our PCM based test calculations. The same methods were utilized to derive the molecular geometries in vacuum. The Gaussian 03 program[34] was used for all geometry optimizations.

The force fields used in the MD simulations consist of partial point charges, isotropic polarizabilities, and LJ parameters. The charges were calculated by fitting to the quantum-mechanical electrostatic potential according to the CHelpG algorithm[35] at the B3LYP/aug-cc-pVTZ level for pyridine and coumarin 151, and the B3LYP/aug-cc-pVDZ level for coumarin 153 in vacuum using the Gaussian 03 program.[34] To model induction interactions, we assigned isotropic polarizabilities to the atomic sites of the solutes. The distributed polarizabilities were computed using the LoProp method[36] available in the Molcas program[37] at the B3LYP/aug-cc-pVTZ level for pyridine and coumarin 151 and the B3LYP/aug-cc-pVDZ level for coumarin 153. The Dunning basis sets were recontracted so as to be of atomic natural orbital type as required by the LoProp method. The LJ parameters for pyridine were taken from ref 38. For both coumarin molecules we used the LJ parameters from the optimized potential for liquid simulations (OPLS) force field given in ref 39, except for the amino group in coumarin 151 where we used the OPLS parameters from ref 40. The water molecules were modeled using the polarizable force field of Ahlström et al.,[41] which represents a water molecule by three atomic point charges and an isotropic molecular polarizability located at the center of mass. The internal geometry of the water molecules was fixed to $R_{OH} = 0.9572$ Å and $\angle HOH = 104.49°$. The geometries of the solvated molecules and force field parameters for pyridine, uracil, coumarin 151, and coumarin 153 as used in the MD simulation are available as Supporting Information.

The MD simulations of a rigid solute molecule, i.e., either pyridine, coumarin 151, or coumarin 153, and 511 rigid water molecules were performed within the NVT ensemble at the temperature of 298.15 K. The cubic box length was always set so as to reproduce the experimental density of liquid water—24.91, 25.05, and 25.12 Å for pyridine, coumarin 151 and coumarin 153, respectively. The velocity Verlet integration algorithm was employed with the time step of 2 fs along with periodic boundary conditions. The electrostatic and LJ interactions were truncated at half of the box length, and the reaction field correction was applied beyond this cutoff. The induced dipole moments were recalculated every third time step with the relative tolerance of 10^{-7}. In addition, the linear damping of the dipole−dipole interactions was employed.[28] Lorentz−Berthelot rules were applied for the LJ interactions of unlike atoms.[42] The system was equilibrated for 200 ps, and the molecular configurations were recorded every 10th ps during the production run of 1.2 ns. We thus have 120 molecular snapshots from each of the MD runs to use in the PE-DFT calculations. All MD simulations were performed using the Molsim software.[43]

4.2. Electronic Structure Calculations. We used the CAM-B3LYP hybrid exchange-correlation functional[44] to compute the excitation energies. This functional exhibits improved long-range behavior which is due to the splitting of the $1/r$ operator into short- and long-range contributions in the exact HF exchange term. The CAM-B3LYP functional has been shown to provide improved results for long-range properties including excitation energies.[44−46] Furthermore, we recently demonstrated that the CAM-B3LYP based solvent shifts of the $\pi \rightarrow \pi^*$ type excitation energies are more reliable as compared to the corresponding B3LYP results.[17,30] The parametrization of the CAM-B3LYP functional as proposed in the original work[44] was used. For all molecules,

except coumarin 153, the aug-cc-pVDZ basis set was used in the calculations of excitation energies, which is adequate for local n → π^* and $\pi \rightarrow \pi^*$ excitation energies.[17,30,47] A smaller 6-31++G* basis[48] was used in the calculations on coumarin 153.

To model the solvent molecules, we used PE potentials based on a hierarchy of force fields computed using the LoProp approach.[36] The force field parameters, i.e., multipole moments and polarizabilities, were derived at the B3LYP/aug-cc-pVTZ level of theory in vacuum using the Molcas program. In this work we use the designation M*X*P*Y* for the force fields, where *X* denotes the highest order of the multipole moments and *Y* indicates whether it includes isotropic ($Y = 1$) or anisotropic ($Y = 2$) polarizabilities. All these parameters are attributed to the atomic sites of the water molecules. In addition to the M*X*P*Y* force fields we also used a force field denoted M2P2BM, which includes multipoles up to quadrupoles and anisotropic polarizabilities assigned to both atomic sites and bond midpoints. Furthermore, we derived a series of force fields using the PCM model which we denote M*X*PCM. In this case the induction effects are incorporated implicitly into the multipole moments. The parameters for these force fields were calculated at the B3LYP/aug-cc-pVTZ/PCM level. Finally, we used the Ahlström force field presented in the previous section and the standard nonpolarizable TIP3P force field due to Jorgensen.[49] The LoProp based force fields are provided in the Supporting Information.

The PE-DFT results for the excitation energies are the statistical averages over 120 molecular configurations. A spherical cutoff radius equal to 12 Å based on the distance between the center of masses of the solute and solvent molecules was used for every configuration. We have previously shown that this cutoff radius provides converged results in terms of electrostatics and that 120 molecular configurations used in the averaging of the liquid-phase results represents statistically converged properties (see, for example, refs 17 and 30). The standard error of the mean is evaluated as $s/\sqrt{N}$, where s is the sample standard deviation and N is the number of samples.

4.3. Benchmarks of the Force Fields. In this work we assess the quality of the force fields used for the water molecules by comparing the molecular electrostatic potentials in the vicinity of the molecule on the basis of the force field and quantum chemical reference calculations. The electrostatic potential is the most suitable observable for such a comparison since it enters directly in the PE potential operator in eq 8. The electrostatic potential was probed at a number of points forming the grid around the water molecule. The grid is formed between two concentric van der Waals surfaces of the molecule. The inner boundary of the grid is a conventional van der Waals surface of water molecule constructed from atom-centered interlocking spheres with the van der Waals radii of 1.55 Å for oxygen[50] and 1.20 Å for hydrogen[51] atoms. The outer boundary is obtained as the van der Waals surface formed using van der Waals radii scaled by a factor of 4. The grid points are then homogeneously distributed between the two van der Waals surfaces with a separation between two neighboring grid points of 0.2 Å in all three directions. The resulting grid is thus composed of 122 263 points in total. The electrostatic potential due to the multipoles at the ath grid point was calculated according to

$$\varphi_a = \sum_{s=1}^{S} \sum_{k=0}^{K} \frac{(-1)^k}{k!} \mathbf{T}_{as}^{(k)} \mathbf{Q}_s^{(k)} \tag{39}$$

where the summations are over all multipole expansion centers in the molecule and all multipoles. The QM electrostatic potential at the ath grid point is the expectation value of the $1/(|\mathbf{r}_a - \mathbf{r}|)$ operator plus the nuclear contribution. The B3LYP exchange-correlation functional and the aug-cc-pVTZ basis set, i.e., the same method used to derive the LoProp force fields, was used to evaluate the QM reference electrostatic potential. The analysis is then performed in terms of the root-mean-square deviation (rmsd)

$$\mathrm{rmsd} = \sqrt{\frac{1}{N} \sum_a (\varphi_a - \varphi_a^{\mathrm{QM}})^2} \tag{40}$$

where N is the number of grid points. In particular, we performed the analysis on the subsets of the grid points between two close-lying van der Waals surfaces so as to investigate the behavior of the rmsd with respect to the distance from the molecule.

The quality of the polarizabilities can be assessed by applying an external homogeneous electric field in the calculation of the electrostatic potential. This field will give rise to induced dipoles which in turn creates an electrostatic potential around the molecule. Two calculations are then performed at the B3LYP/aug-cc-pVTZ level—one in vacuum and another in the external electric field. The QM reference is then obtained by subtracting the electrostatic potential in vacuum from that in the external field at every grid point. In this work we applied an electric field with the magnitude of 0.01 a.u. and all Cartesian components positive and equal. We used the Dalton program for the QM calculations, whereas the construction of the grid, calculations of the electrostatic potential and the analysis are performed using the Whirlpool program.[52]

5. Results and Discussion

Below we detail the results from the calculations performed using the PE-DFT approach with regards to the assessment of the force fields.

5.1. Quality of the Force Fields. We inspect the quality of the force fields used for a water molecule by comparing the electrostatic potentials due to classical and quantum mechanical representations of the molecule. This is important in the present context as it is desirable to use, for example, permanent multipole expansions truncated at the lowest possible order and still obtain converged electrostatic interactions. Similarly, it is of interest to investigate if the induction effects are sufficiently accurately described by using the simpler isotropic form of the polarizabilities or if anisotropic polarizabilities have to be used. The distribution of the force field parameters over the molecule is also an open question.

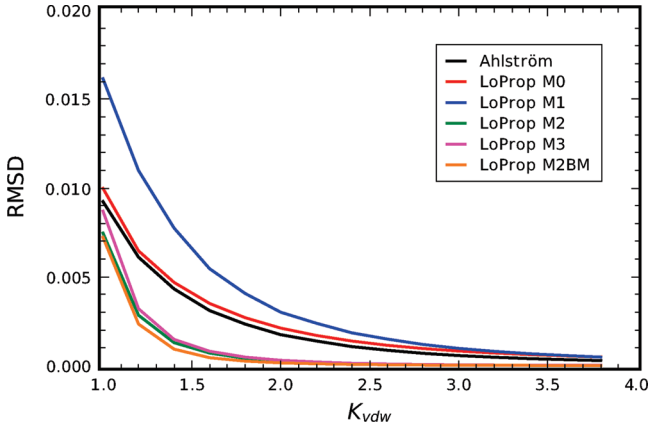

Figure 1. rmsd of the molecular electrostatic potential due to the multipoles of a water molecule as a function of the distance from the molecular van der Waals surface. The distance from the surface is given as the factor scaling the van der Waals radii. rmsd is in a.u.

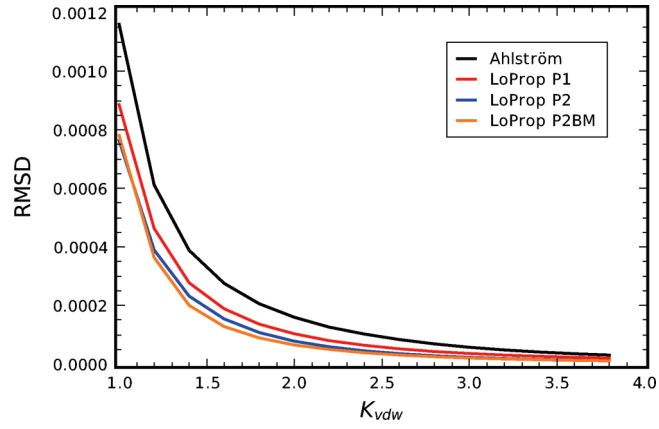

Figure 2. rmsd of the molecular electrostatic potential due to the induced dipole moments of a water molecule as a function of the distance from the molecular van der Waals surface. The distance from the surface is given as the factor scaling the van der Waals radii. rmsd is in a.u.

In Figure 1 we show the rmsd obtained by comparing the molecular electrostatic potential due to multipole moments taken from the considered force field and the quantum mechanically computed potential for different distances from the molecular van der Waals surface. In particular, we consider the three atomic point charges from the Ahlström force field and multipoles up to octupoles taken from the LoProp force fields. Figure 1 clearly illustrates that the multipole expansion is appropriate at large distances from the molecule and that higher order multipoles are mandatory to consider when the molecular potential close to the molecule is probed. We observe that the electrostatic potential due to the LoProp force field including atomic charges and dipole moments (M1) is poorer recovered than using the atomic point charges (M0) only. Quadrupole moments have a very pronounced effect and improve the molecular electrostatic potential considerably, as it was also found in ref 53. The octupole moments contribute little to the electrostatic potential. The atomic point charges in the Ahlström force field are constructed so as to implicitly include higher order multipoles. However, it is evident from Figure 1 that the improvement is negligible compared to the M0 force field and cannot match the performance of the M2 force field. We see that the LoProp force field which includes multipoles at bond midpoints (M2BM) offers minor improvement as well. We also inspected the M3BM force field, and octupoles were found to provide virtually no improvement. To conclude, we find that the LoProp force field with multipoles up to quadrupole moments assigned to the atomic sites of the water molecule provides apparently converged electrostatic interactions in terms of the multipole expansion.

In Figure 2 we compare the induced changes in the electrostatic potentials due to an external electric field. Here the electrostatic potential is due to the dipole moments induced by the external electric field. The QM reference electrostatic potential is the difference between the potential with and without the external field. We observe that the distributed isotropic polarizabilities in the LoProp force field lead to a more accurate account of the polarization of the electrostatic potential as compared to the single molecular isotropic polarizability assigned to the oxygen site of the water molecule in the Ahlström force field. Further improvement, though not that pronounced, is achieved by using the anisotropic polarizabilities. However, we would expect a larger difference in other molecules with a higher degree of anisotropy than a water molecule. We note that the rmsd in the case of induced dipoles is smaller by at least an order of magnitude than that due to the multipoles. This indicates that the specific description of the polarization is not as important as an accurate account of the electrostatics. However, as detailed later, explicit inclusion of polarization is generally found to be important for solvent induced shifts of excitation energies.

5.2. Excitation Energies. We examine the effects from the water solvent on the excitation energies of the solute molecules using our PE-DFT method. More precisely, we will look at the behavior of the solvent induced shifts of the excitation energies as we vary the complexity of the force field used in the PE-DFT calculations. We only include a solute molecule in the QM core; thereby only electrostatic and induction interactions are considered even though other interactions are known to be important, especially for $\pi \rightarrow \pi^*$ transitions.[17,30] This allows us to systematically investigate the effects from the electrostatic and induction interactions on the solvent shifts.

The computed excitation energies used as gas-phase references for the solvent shifts are shown in Table 1 together with the corresponding experimental data.[54−58] The computed excitation energies are generally in good agreement with the experimental values. For the $n \rightarrow \pi^*$ transitions the calculated values are off by 0.01 and 0.1 eV for acetone and acrolein, respectively. In the case of $\pi \rightarrow \pi^*$ transitions the deviation from experiment ranges from 0.02 eV in acrolein to 0.6 eV in pyridine. For uracil and the coumarins the computed excitation energies are overestimated by about 0.3 eV. It should be noted that the presented experimental value for coumarin 151 is our estimate of the excitation energy at the absorption maximum in vapor phase. It is based on values given by Ernsting et al.[58] In that work the authors measured the wavelengths of the absorption maxima of several

Table 1. Calculated and Experimental Gas-Phase Reference Vertical Excitation Energies of the Lowest $n \rightarrow \pi^*$ and/or $\pi \rightarrow \pi^*$ Transitions[a]

	ΔE_{vac} (eV)	
	calcd	exptl
n $\rightarrow \pi^*$		
acetone	4.473[b]	4.46[e]
acrolein	3.783[c]	3.69[f]
$\pi \rightarrow \pi^*$		
acrolein	6.405[c]	6.42[f]
pyridine	5.595	4.99[g]
uracil	5.384[d]	5.08[h]
coumarin 151	4.020	3.81 ± 0.06[i]
coumarin 153	3.675	3.37[j]

[a] The calculations were performed at the CAM-B3LYP/aug-cc-pVDZ level. [b] Reference 29. [c] Reference 17. [d] Reference 30. [e] Reference 54. [f] Reference 55. [g] Reference 56. [h] Reference 57. [i] Estimated value based on experimental data in ref 58 (see section 5.2 for more details). [j] Reference 58.

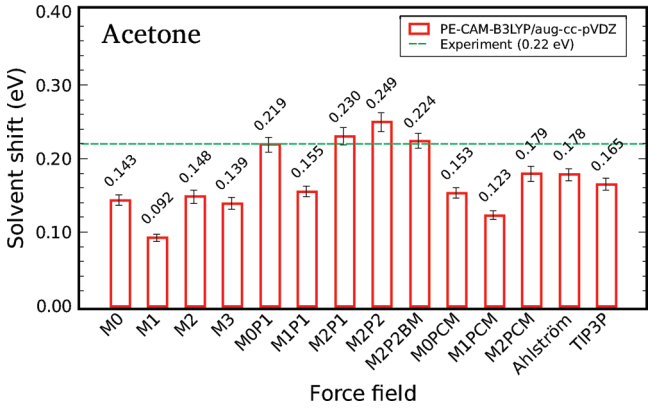

Figure 3. Gas-to-aqueous solvent shift of the lowest n $\rightarrow \pi^*$ excitation energy in acetone.

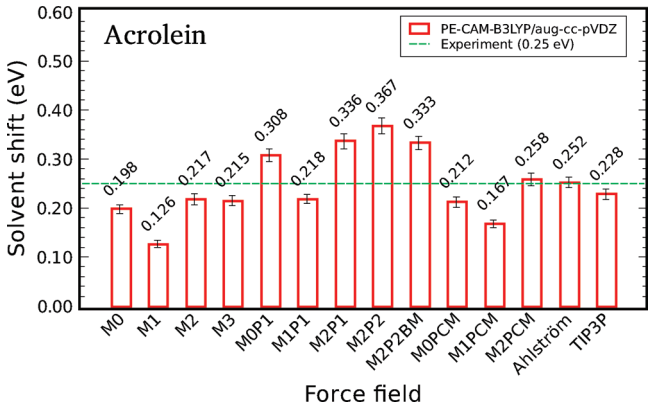

Figure 4. Gas-to-aqueous solvent shift of the lowest n $\rightarrow \pi^*$ excitation energy in acrolein.

coumarins and also the first strong vibronic band observed in a supersonic jet. The difference between the wavelengths of the absorption maxima and the vibronic bands are between about 18 and 28 nm. Subtracting the differences from the measured vibronic band of coumarin 151 leads to our estimate of the excitation energy at the absorption maximum in vapor phase given in the table.

The calculated solvent shifts are shown in Figures 3−9 together with the experimental solvent shift.[54−61] The first columns, i.e., M0, M1, M2 and in the cases of acetone,

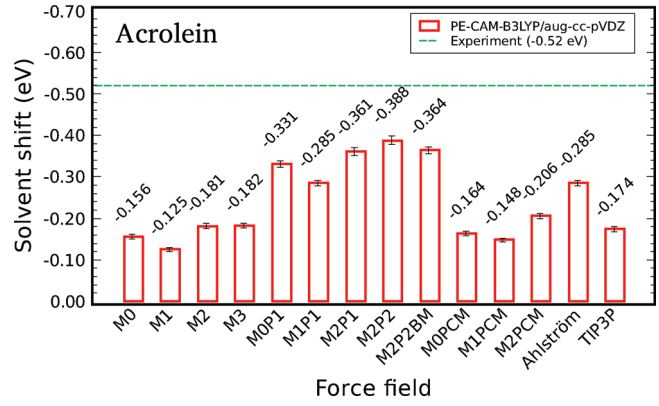

Figure 5. Gas-to-aqueous solvent shift of the lowest $\pi \rightarrow \pi^*$ excitation energy in acrolein.

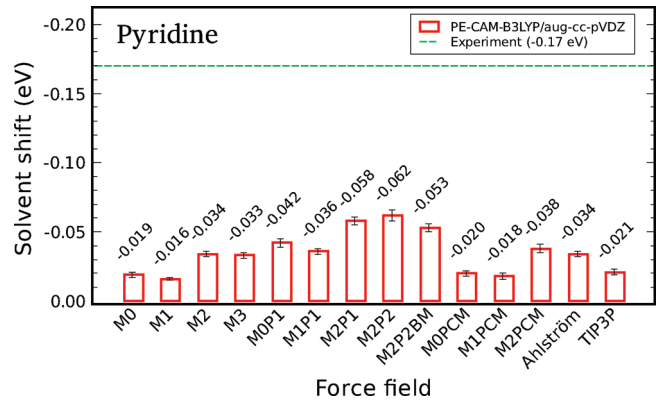

Figure 6. Gas-to-aqueous solvent shift of the lowest $\pi \rightarrow \pi^*$ excitation energy in pyridine.

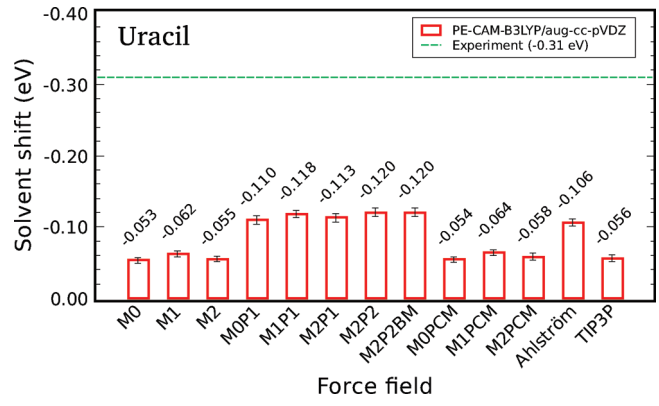

Figure 7. Gas-to-aqueous solvent shift of the lowest $\pi \rightarrow \pi^*$ excitation energy in uracil.

acrolein, and pyridine also M3, in each figure show the trends of the shifts with increasing order of the multipole expansion. These force fields do not model solvent polarization and are only used to investigate the effects of the higher order multipoles on the excitation energies. In all cases we observe a large effect from both the dipole and quadrupole moments. Adding octupoles only leads to very small changes that are within the statistical errors, indicating that we are converged at the quadrupole level with respect to the order of the permanent multipole moments. We thus observe a clear correlation between the trends here and the behavior of the force fields in terms of how well they reproduce the QM electrostatic potential (see Figure 1 and discussion in section

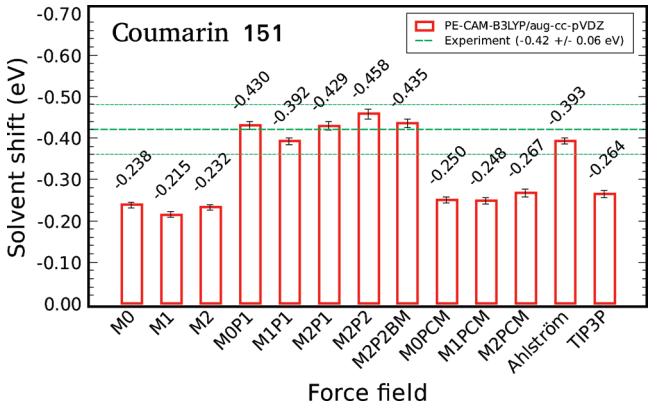

Figure 8. Gas-to-aqueous solvent shift of the lowest $\pi \rightarrow \pi^*$ excitation energy in coumarin 151.

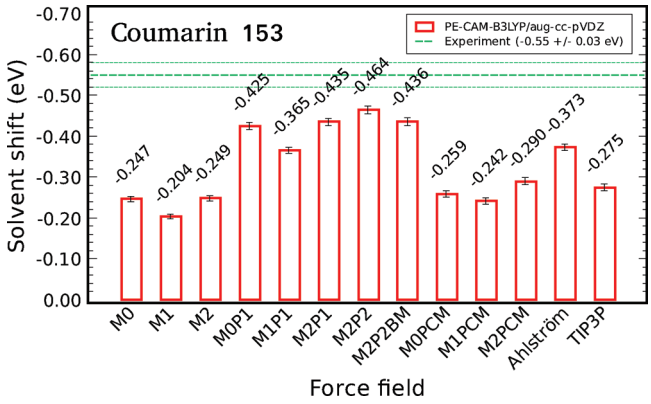

Figure 9. Gas-to-aqueous solvent shift of the lowest $\pi \rightarrow \pi^*$ excitation energy in coumarin 153.

5.1). Note that the shifts at the M0 and M2 (and M3) levels in general are very similar due to the fact that the effects from the dipole and quadrupole moments tend to cancel each other. This is not always the case, however, as we clearly see for pyridine (Figure 6) where the shifts at the M2 (and M3) level are about 75% larger than at the M0 level and, less pronounced, in acrolein (Figures 4 and 5) where the same difference is about 10 and 15%, respectively. Finally, we note that the same tendencies are observed in the M0P1−M2P1 and M0PCM−M2PCM series of force fields. Therefore, we find that it is, in general, necessary to include permanent multipoles up to quadrupoles in the LoProp force fields to get a converged description of the electrostatic interactions. However, using only point charges can, in some cases, lead to satisfying results as well.

Introducing distributed isotropic polarizabilities, in addition to the permanent multipoles, to the LoProp force fields, i.e., M0P1, M1P1, and M2P1, leads to a substantial increase of the solvent shifts. Comparing the shifts calculated at the M2P1 level to the M2 level shows that the solvent shifts are increased from about 50% in the case of $n \rightarrow \pi^*$ transitions in acetone (Figure 3) and acrolein (Figure 4) to more than 100% for the $\pi \rightarrow \pi^*$ transition in uracil (Figure 6). This clearly shows that induction effects have a significant impact on the solvent shifts and therefore must be taken into account. Furthermore, we observe that induction effects are particularly important for $\pi \rightarrow \pi^*$ transitions. Using distributed anisotropic polarizabilities, i.e., the M2P2 force field, gives further 6−10% increase in the solvent shifts as compared to the M2P1 level, which in the case of pyridine and uracil is about the same size as the statistical errors. Thus, the use of distributed anisotropic polarizabilities only gives small improvements as compared to the distributed isotropic polarizabilities. This can be explained by a rather small degree of anisotropy of a water molecule. Using the most sophisticated LoProp force field, M2P2BM, decreases the solvent shifts by a small amount as compared to the M2P2 force field which is of comparable magnitude but opposite sign as the difference between the M2P1 and M2P2 force fields. This indicates that the M2P2 force field has a tendency to overestimate the induction effects. Furthermore, it shows that it can be sufficient to use the M2P1 force field; however, this is only true for solvent molecules with low anisotropy such as water. The improved results at the M2P2BM level can mainly be contributed to an improved description of the induction interactions since we expect that the electrostatic interactions are converged at the quadrupole level. We expect that the M2P2BM force field provides the best model of the environment through an elaborate description of both the electrostatic and induction effects. This is achieved by using a converged distributed multipole expansion and distributed anisotropic polarizabilities with all properties localized on atoms and bond midpoints. It is interesting that the M0P1 force field performs rather well in most cases compared to the full M2P2BM force field. Therefore, we find that an appropriate approximation of the PE potential would be to use the M0P1 force field which captures the main parts of the electrostatics and induction effects due to a water solvent on the vertical excitation energies.

Recognizing that it is necessary to include the induction effects, it is an open question whether explicit inclusion of polarization is mandatory or if it is sufficient to have implicit polarization by using enhanced permanent multipoles. We used the PCM method in combination with the LoProp method to model the bulk solvent effects on the permanent multipoles. Using the M0PCM, M1PCM, and M2PCM force fields, we obtained larger solvent shifts as compared to the M0, M1, and M2 force fields. However, at the point charge level this increase is comparable to the statistical errors. Therefore, to obtain an improved description of the environment using the LoProp method in combination with PCM, it is necessary to include multipoles up to quadrupoles, i.e., the M2PCM force field. Here it appears that the largest effect is achieved for $n \rightarrow \pi^*$ transitions, which indicates that explicit modeling of induction effects are important for $\pi \rightarrow \pi^*$ transitions. The results for the solvent shifts of the $n \rightarrow \pi^*$ transitions calculated using the M2PCM force field are about 20% smaller than the shifts obtained using the M2P2BM force field. For the $\pi \rightarrow \pi^*$ transitions this difference is even larger and ranges from roughly 30 to 50%. Therefore, we find that the nonpolarizable M2PCM force field can be a reasonable representation of water molecules when $n \rightarrow \pi^*$ transitions are considered depending on the desired accuracy. However, explicit treatment of polarization is essential for $\pi \rightarrow \pi^*$ transitions.

It is interesting to compare the results obtained using the elaborate LoProp force field, M2P2BM, with other com-

Table 2. Comparison of Solvent Shifts Where the Environmental Response Due to the Differential Change between the Ground- and Excited-State Electron Density Is Approximated (See Section 5.2 for Details)[a]

solute	Q_1	Q_2^*	Q_2
acetone ($n \rightarrow \pi^*$)	0.226	0.224	0.224
coumarin 151 ($\pi \rightarrow \pi^*$)	−0.353	−0.451	−0.435

[a] The calculations were performed at the PE(M2P2BM)-CAM-B3LYP/aug-cc-pVDZ level.

Table 3. Molecular Dipole Moments of Solvated Acetone and Coumarin 151 in the Ground State and Excited States Corresponding to the Lowest $n \rightarrow \pi^*$ and $\pi \rightarrow \pi^*$ Transitions in Acetone and Coumarin 151, Respectively[a]

solute	μ^{gs} (D)	μ^{ex} (D)
acetone	5.0	3.7
coumarin 151	11.0	15.8

[a] The calculations were performed at the PE(M2P2BM)-CAM-B3LYP/aug-cc-pVDZ level.

monly used force fields. For this purpose we chose the standard nonpolarizable TIP3P force field and the polarizable Ahlström force field. The solvent shifts obtained using the TIP3P force field are all significantly smaller than those obtained using the M2P2BM force field. As expected we also observe substantially larger deviations for the $\pi \rightarrow \pi^*$ transitions since these require explicit modeling of the induction effects. The shifts of the $n \rightarrow \pi^*$ transitions are about 20% smaller compared to the results obtained using the M2P2BM force field, whereas the shifts of the $\pi \rightarrow \pi^*$ transitions vary between roughly 40 and 60%. The Ahlström force field, on the other hand, provides results that are in much better agreement with the results computed using the M2P2BM force field. Using this force field results in shifts that are about 10−35% smaller as compared to the M2P2BM level.

It is common to neglect the dynamical response of the environment that is due to the differential change between the ground-state and excited-state electron density or to include it in an approximate form.[7,8] We will denote the first case as the Q_1 approximation because it corresponds to the neglect of the $\hat{Q}_2^{\omega}$ operator (eq 21) in the case of linear response. The second case we will denote as the Q_2^* approximation, where the $\hat{Q}_2^{\omega}$ operator is included in an approximated form which corresponds to a block-diagonal classical response matrix (eq 6) with the polarizability tensors along the diagonal; i.e., the interaction tensors are omitted. In the Q_1 approximation the induced dipoles from the optimization of the ground-state wave function are also used in the response calculations. This can be a good approximation if the electronic density of the solute does not change significantly upon excitation. The Q_2^* approximation partly captures the dynamical environmental response, and the size of the effect is also connected to the difference between the electronic densities of the ground and excited states. To examine the effects of both approximations, we made additional calculations on acetone and coumarin 151. The results can be found in Table 2, where the Q_1 column presents the solvent shifts using the Q_1 approximation and the Q_2^* column contains the results where the Q_2^* approximation is used and in the final Q_2 column are the shifts where the full dynamical response of the environment is included. First of all we observe that both approximations have negligible or no effect on the $n \rightarrow \pi^*$ transition in acetone compared to the full inclusion of dynamical response. However, for the $\pi \rightarrow \pi^*$ transition in coumarin 151 we observe substantial effects from the Q_1 approximation and to a lesser degree from the Q_2^* approximation. The Q_1 approximation results in a solvent shift that is roughly 20% smaller than the shift calculated without approximations, while the Q_2^* approximation overshoots by roughly 4%. As a measure of the difference between the electron density of the ground and excited states we also calculated the difference between the dipole moment of the ground and excited states of acetone and coumarin 151 in aqueous solution at the PE(M2P2BM)-CAM-B3LYP/aug-cc-pVDZ level. This quantity is conveniently obtained as the residue of a quadratic response function. The calculated dipole moments are shown in Table 3. Here we see that the magnitude of the dipole moment of acetone decreases by 1.3 D upon excitation, whereas in coumarin 151 it goes up by 4.8 D thus explaining the much larger effects due to the Q_1 and Q_2^* approximations on the $\pi \rightarrow \pi^*$ transition in coumarin 151. These results clearly show that completely neglecting the dynamical response of the environment when computing excitation energies is a severe approximation if there is a significant change in the electron density upon excitation. The results also indicate that the approximate inclusion of dynamical response is a much better approximation; however, the error is still significant compared to the statistical errors. Moreover, we would expect the error to become larger in molecular systems where the difference of the ground- and excited-state electron density is even larger.

The $n \rightarrow \pi^*$ electronic absorption energies of acetone and acrolein have been extensively studied using different theoretical solvation models, and we refer to refs 17, 47, and 62 and references therein for discussion of some previously reported results. Very recent experimental measurements by Renge[54] estimate the gas-to-aqueous solvent shift of the $n \rightarrow \pi^*$ transition in acetone at 0.22 eV. The experimental estimate of the corresponding solvent shift in acrolein of 0.25 eV[55] has recently been confirmed.[17] Yoo et al.[8] used DFT in combination with the EFP method to compute the solvent shift of acetone, and the resulting shift of 0.21 eV compares very well to experimental result. Very recently, Kaminski et al.[63] have used the orbital-free embedding potential due to the statistically averaged solvent density through three-dimensional reference interaction site model (OFE/RISM) to study the lowest excitation energies of several organic probes in solution. The computed gas-to-aqueous solvent shift of the $n \rightarrow \pi^*$ transition in acetone is 0.19 eV, while the corresponding shift in acrolein of 0.33 eV is found to be somewhat overestimated compared to experimental data. Recently, several studies have elucidated the $n \rightarrow \pi^*$ transition in acetone and/or acrolein in water solution using electronic structure approaches rooted in coupled cluster theory. Caricato et al.[64] have evaluated this solvent shift in acrolein using EOM-CCSD/PCM and obtained 0.23 eV. A solvent shift of 0.18 eV in acetone was predicted on the basis of CCSD/MM calculations using a

Table 4. Calculated and Experimental Vertical Excitation Energies of the Lowest $n \rightarrow \pi^*$ and/or $\pi \rightarrow \pi^*$ Transitions in the Solvated Molecules[a]

	ΔE_{aq} (eV)	
	calcd	exptl
$n \rightarrow \pi^*$		
acetone	4.697 ± 0.010	4.68[b]
acrolein	4.116 ± 0.014	3.94[c]
$\pi \rightarrow \pi^*$		
acrolein	6.041 ± 0.009	5.90[c]
pyridine	5.542 ± 0.003	4.82[d]
uracil	5.264 ± 0.006	4.77[e]
coumarin 151	3.585 ± 0.011	3.39[f]
coumarin 153	3.239 ± 0.010	2.82 ± 0.03[g]

[a] The calculations were performed at the PE(M2P2BM)-CAM-B3LYP/aug-cc-pVDZ level. [b] Reference 54. [c] Reference 55. [d] Reference 59. [e] Reference 57. [f] Reference 60. [g] Value measured on a spectrum of coumarin 153 in aqueous 1-propanol solution ($X_{PrOH} = 0.05$) provided in ref 61.

nonpolarizable water potential.[65] Mata[66] has investigated the many-body effects on the solvent shifts and obtained 0.12 and 0.24 eV for the solvent shifts of acetone and acrolein, respectively, using a reduced two-body expansion with the EOM-CCSD method. Sneskov et al.[67] have elucidated the importance of triples excitations in the coupled cluster expansion on the solvent shift of the $n \rightarrow \pi^*$ and $\pi \rightarrow \pi^*$ excitation energies of acrolein and have found generally small effects as compared to CCSD. This short overview of the most recent results demonstrates the capability of different theoretical methods to describe the solvent effects on the $n \rightarrow \pi^*$ transition of acrolein and acetone. In this work we have observed a satisfactory agreement between theoretical and experimental results for the solvent shifts of the $n \rightarrow \pi^*$ transition of acetone. However, the solvent shift of 0.33 eV for acrolein is overestimated as compared to the experimentally measured 0.25 eV. The experimental data[54,55,57,59−61] for the solutes in aqueous solution are provided in Table 4 together with the corresponding theoretical values obtained using the M2P2BM force field.

Nonelectrostatic interactions have been found to substantially contribute to the solvent shift of the $\pi \rightarrow \pi^*$ transitions.[17,30,66] In this study we have neglected all effects other than electrostatic and induction interactions, and therefore the computed solvent shifts of the $\pi \rightarrow \pi^*$ excitation energies are in general considerably underestimated against experimental data, as illustrated in Figure 5 to Figure 9. Calculations by Caricato et al.[64] using EOM-CCSD and PCM gave a solvent shift of −0.38 eV of the $\pi \rightarrow \pi^*$ transition in acrolein, which is very similar to the results of the present work and also to the results based on CCSDR(3)/MM calculations in ref 67. In ref 66 the EOM-CCSD method coupled to the TIP3P force field for the water molecules gave a solvent shift of −0.27 eV in acrolein. Furthermore, extensive two-body expansions were found to be mandatory to obtain good agreement with experimental data. High-level coupled-cluster calculations have estimated a blue-shift of the $\pi \rightarrow \pi^*$ transition in uracil.[68] In that work, a gas-phase result which is in much better agreement with experiment, was obtained; however, the effects from the solvent are not well described which emphasizes the importance of a good embedding potential, especially when considering $\pi \rightarrow \pi^*$ transitions. Very recent CC2/MM calculations using the Ahlström force field predicted the solvent shift of −0.20 eV.[30] In the present paper a smaller shift of around −0.11 eV was found, indicating that in this case the CC2 model accounts more accurately for the differential effects of dynamical correlation compared to the CAM-B3LYP functional. A solvent shift of −0.25 eV in coumarin 151 was obtained from OFE/RISM calculations,[63] which is somewhat underestimated as compared to our PE-DFT results and experimental estimate. Sulpizi et al.[69] have obtained a solvent shift of −0.33 eV for coumarin 153 from TD-DFT/MM simulations which is somewhat smaller compared to our predictions and experimental findings, likely due to the implicit treatment of intermolecular polarization.

6. Summary and Conclusions

We have presented the theoretical details and implementation of the PE-DFT (and PE-HF) method. This method is a focused model based on a self-consistent polarizable embedding scheme, i.e., the PE model, applied to Kohn−Sham density functional theory. The method includes ground-state density optimization and calculation of molecular properties through time-dependent response theory, wherein the effects from a polarizable atomistic environment are taken into account in a self-consistent manner. The electrostatic interactions are modeled using a multicenter multipole expansion which includes multipoles up to and including octupoles. The polarization of the environment is described by using distributed anisotropic polarizability tensors. The multipoles and polarizability tensors are derived from quantum mechanical calculations and are distributed on the atomic sites or on the atomic sites and bond midpoints.

To evaluate the performance of the method, we benchmarked a series of force fields for a water molecule. The electrostatic potential due to the permanent multipole moments was sampled and compared to the quantum mechanically derived electrostatic potential. We found that the multipole expansion converges at the quadrupole level where it performs well at long and medium distances compared to the reference electrostatic potential. The errors increase at short distances but still show a big improvement compared to force fields with multipole moments truncated at lower order. The electrostatic potential due to induced dipole moments was also benchmarked and showed that the contribution from induction effects to the electrostatic potential is small compared to the permanent multipole moments. The best performance was observed with distributed anisotropic polarizabilities, although the improvement over distributed isotropic polarizabilities was not impressive. This was ascribed to the low degree of anisotropy of a water molecule.

The capability of the implemented method was demonstrated by computing the gas-to-aqueous solvent induced shifts of the lowest $n \rightarrow \pi^*$ vertical excitation energy in acetone and acrolein and the lowest $\pi \rightarrow \pi^*$ vertical excitation energy in acrolein, pyridine, uracil, coumarin 151, and coumarin 153. The solute−solvent dynamics were taken into account through classical molecular dynamics simulations

using polarizable force fields. A systematic investigation of the effects from electrostatic and induction interactions on the solvent shifts showed that the effects on the solvent shifts from electrostatic interactions converge at the quadrupole level, consistent with the benchmarking of the force fields. Furthermore, we found that modeling of the induction interactions is essential for the calculation of accurate solvent shifts, particularly for $\pi \rightarrow \pi^*$ transitions. The best performance was observed with the most detailed force field which includes multipoles up to quadrupoles and anisotropic polarizability tensors distributed on atomic sites and bond midpoints of the water molecules. Including the induction effects implicitly through an enhancement of the permanent multipole moments improved the solvent shifts although it could not match the results where explicit modeling was used. Moreover, for $\pi \rightarrow \pi^*$ transitions the effects were rather small and we therefore found that explicit account of the induction interactions is necessary for excitations of this nature. Finally, we found that an appropriate approximation of a water solvent should as a minimum consist of point charges and isotropic polarizabilities, which capture the main parts of the electrostatics and induction effects on the vertical excitation energies.

Our formulation of polarizable embedding within response theory includes the fully self-consistent many-body response of the environment. We investigated the effects on the solvent shifts when the dynamical response of the environment due to the differential change between the ground- and excited-state electron density is either neglected or approximated. Both are valid approximations if the electron density does not change significantly upon excitation. Calculations on acetone and coumarin 151, which have a small and large difference, respectively, between the dipole moment of the ground and relevant excited state, showed that complete neglect of the dynamical response can introduce significant errors. For coumarin 151 it comprised as much as 20% of the total calculated shift. The error due to an approximate inclusion of the dynamical environmental response was only 4% of the total shift in coumarin 151 and therefore presents a much better approximation. These errors are expected to increase in molecular systems where the electron density difference between the ground and excited states becomes even larger.

Comparisons with experiment showed satisfactory agreement. The sign of the solvent shifts, i.e., blue shift of $n \rightarrow \pi^*$ transitions and red shift of $\pi \rightarrow \pi^*$ transitions, were in all cases correctly predicted. For $n \rightarrow \pi^*$ transitions the solvent shifts tend to be slightly overestimated while the opposite applied to $\pi \rightarrow \pi^*$ transitions. This was ascribed to the neglect of certain intermolecular interactions, e.g., short-range repulsion and dispersion, as well as the limitations inherent in current exchange-correlation functionals.

Acknowledgment. We thank the Danish Center for Scientific Computing for the computational resources. J.K. thanks the Danish Natural Science Research Council/The Danish Councils for Independent Research for financial support.

Supporting Information Available: Tables showing solvated molecular geometries and force field parameters for pyridine, coumarin 151, and coumarin 153, the parameters of the water molecules as used in the MD simulation, LoProp based force fields, and Ahlström and TIP3P force fields used for the water molecules in the PE-DFT calculations. This material is available free of charge via the Internet at http://pubs.acs.org.

References

(1) van Mourik, T. *Philos. Trans. R. Soc. London, A* **2004**, *362*, 2653.

(2) Ochsenfeld, C.; Kussmann, J.; Lambrecht, D. S. *Rev. Comput. Chem.* **2007**, *23*, 1.

(3) Applequist, J.; Carl, J. R.; Fung, K.-K. *J. Am. Chem. Soc.* **1972**, *94*, 2952.

(4) Day, P. N.; Jensen, J. H.; Gordon, M. S.; Webb, S. P.; Stevens, W. J.; Krauss, M.; Garmer, D.; Basch, H.; Cohen, D. *J. Chem. Phys.* **1996**, *105*, 1968.

(5) Gordon, M. S.; Freitag, M. A.; Bandyopadhyay, P.; Jensen, J. H.; Kairys, V.; Stevens, W. J. *J. Phys. Chem. A* **2001**, *105*, 293.

(6) Gordon, M. S.; Slipchenko, L. V.; Li, H.; Jensen, J. H. *Annu. Rep. Comput. Chem.* **2007**, *3*, 177.

(7) Nielsen, C. B.; Christiansen, O.; Mikkelsen, K. V.; Kongsted, J. *J. Chem. Phys.* **2007**, *126*, 154112.

(8) Yoo, S.; Zahariev, F.; Sok, S.; Gordon, M. S. *J. Chem. Phys.* **2008**, *129*, 144112.

(9) Arora, P.; Slipchenko, L. V.; Webb, S. P.; DeFusco, A.; Gordon, M. S. *J. Phys. Chem. A* **2010**, *114*, 6742.

(10) Slipchenko, L. V. *J. Phys. Chem. A* **2010**, *114*, 8824.

(11) Jorgensen, W. L. *J. Chem. Theory Comput.* **2007**, *3*, 1877.

(12) Yu, H.; van Gunsteren, W. F. *Comput. Phys. Commun.* **2005**, *172*, 69.

(13) McRae, E. G. *J. Phys. Chem.* **1957**, *61*, 562.

(14) Kongsted, J.; Mennucci, B. *J. Phys. Chem. A* **2007**, *111*, 9890.

(15) Pavone, M.; Cimino, P.; De Angelis, F.; Barone, V. *J. Am. Chem. Soc.* **2006**, *128*, 4338.

(16) Brancato, G.; Barone, V.; Rega, N. *Theor. Chem. Acc.* **2007**, *117*, 1001.

(17) Aidas, K.; Møgelhøj, A.; Nilsson, E. J. K.; Johnson, M. S.; Mikkelsen, K. V.; Christiansen, O.; Söderhjelm, P.; Kongsted, J. *J. Chem. Phys.* **2008**, *128*, 194503.

(18) Warshel, A.; Levitt, M. *J. Mol. Biol.* **1976**, *103*, 227.

(19) Singh, U. C.; Kollman, P. A. *J. Comput. Chem.* **1986**, *7*, 718.

(20) Field, M. J.; Bash, P. A.; Karplus, M. *J. Comput. Chem.* **1990**, *11*, 700.

(21) Gao, J.; Xia, X. *Science* **1992**, *258*, 631.

(22) Lin, H.; Truhlar, D. G. *Theor. Chem. Acc.* **2007**, *117*, 185.

(23) Sałek, P.; Vahtras, O.; Helgaker, T.; Ågren, H. *J. Chem. Phys.* **2002**, *117*, 9630.

(24) Olsen, J.; Jørgensen, P. *J. Chem. Phys.* **1985**, *82*, 3235.

(25) Helgaker, T.; Jørgensen, P.; Olsen, J. *Molecular Electronic-Structure Theory*; Wiley: New York, 2000.

(26) DALTON, a molecular electronic structure program, Release 2.0, 2005; see: http://www.kjemi.uio.no/software/dalton/dalton.html.

(27) Thole, B. T. *Chem. Phys.* **1981**, *59*, 341.

(28) van Duijnen, P. T.; Swart, M. *J. Phys. Chem. A* **1998**, *102*, 2399.

(29) Aidas, K.; Møgelhøj, A.; Kjær, H.; Nielsen, C. B.; Mikkelsen, K. V.; Ruud, K.; Christiansen, O.; Kongsted, J. *J. Phys. Chem. A* **2007**, *111*, 4199.

(30) Olsen, J. M.; Aidas, K.; Mikkelsen, K. V.; Kongsted, J. *J. Chem. Theory Comput.* **2010**, *6*, 249.

(31) Becke, A. D. *J. Chem. Phys.* **1993**, *98*, 5648.

(32) Kendall, R. A.; Dunning, T. H.; Harrison, R. J. *J. Chem. Phys.* **1992**, *96*, 6796.

(33) Tomasi, J.; Mennucci, B.; Cammi, R. *Chem. Rev.* **2005**, *105*, 2999.

(34) Frisch, M. J. *Gaussian 03*, Revision B.05; Gaussian: Wallingford, CT, 2004.

(35) Breneman, C. M.; Wiberg, K. B. *J. Comput. Chem.* **1990**, *11*, 361.

(36) Gagliardi, L.; Lindh, R.; Karlström, G. *J. Chem. Phys.* **2004**, *121*, 4494.

(37) Karlström, G.; Lindh, R.; Malmqvist, P.-Å.; Roos, B. O.; Ryde, U.; Veryazov, V.; Widmark, P.-O.; Cossi, M.; Schimmelpfennig, B.; Neogrady, P.; Seijo, L. *Comput. Mater. Sci.* **2003**, *28*, 222.

(38) Jorgensen, W. L.; McDonald, N. A. *J. Mol. Struct. (THEOCHEM)* **1998**, *424*, 145.

(39) Cinacchi, G.; Ingrosso, F.; Tani, A. *J. Phys. Chem. B* **2006**, *110*, 13633.

(40) Pranata, J.; Wierschke, S. G.; Jorgensen, W. L. *J. Am. Chem. Soc.* **1991**, *113*, 2810.

(41) Ahlström, P.; Wallqvist, A.; Engström, S.; Jönsson, B. *Mol. Phys.* **1989**, *68*, 563.

(42) Allen, M. P.; Tildesley, D. J. *Computer Simulation of Liquids*; Clarendon Press: Oxford, U.K., 1987.

(43) Linse, P. *MOLSIM 3.3.0*; Lund University: Lund, Sweden, 2001.

(44) Yanai, T.; Tew, D. P.; Handy, N. C. *Chem. Phys. Lett.* **2004**, *393*, 51.

(45) Peach, M. J. G.; Helgaker, T.; Sałek, P.; Keal, T. W.; Lutnæs, O. B.; Tozer, D. J.; Handy, N. C. *Phys. Chem. Chem. Phys.* **2006**, *8*, 558.

(46) Peach, M. J. G.; Benfield, P.; Helgaker, T.; Tozer, D. J. *J. Chem. Phys.* **2008**, *128*, 044118.

(47) Aidas, K.; Kongsted, J.; Osted, A.; Mikkelsen, K. V.; Christiansen, O. *J. Phys. Chem. A* **2005**, *109*, 8001.

(48) Clark, T.; Chandrasekhar, J.; Spitznagel, G. W.; Schleyer, P. V. R. *J. Comput. Chem.* **1983**, *4*, 294.

(49) Jorgensen, W. L. *J. Am. Chem. Soc.* **1981**, *103*, 335.

(50) Batsanov, S. S. *Inorg. Mater.* **2001**, *37*, 871.

(51) Bondi, A. *J. Phys. Chem.* **1964**, *68*, 441.

(52) Aidas, K. *Whirlpool, a QM/MM Analysis program*, version 1.00; 2010.

(53) Söderhjelm, P.; Krogh, J. W.; Karlström, G.; Ryde, U.; Lindh, R. *J. Comput. Chem.* **2007**, *28*, 1083.

(54) Renge, I. *J. Phys. Chem. A* **2009**, *113*, 10678.

(55) Moskvin, A. F.; Yablonskii, O. P.; Bondar, L. F. *Theor. Exp. Chem.* **1966**, *2*, 469.

(56) Bolovinos, A.; Tsekeris, P.; Philis, J.; Pantos, E.; Andritsopoulos, G. *J. Mol. Spectrosc.* **1984**, *103*, 240.

(57) Clark, L. B.; Peschel, G. G.; Tinoco, I., Jr. *J. Phys. Chem.* **1965**, *69*, 3615.

(58) Ernsting, N. P.; Asimov, M.; Schäfer, F. P. *Chem. Phys. Lett.* **1982**, *91*, 231.

(59) Andon, R. J. L.; Cox, J. D.; Herington, E. F. G. *Trans. Faraday Soc.* **1954**, *50*, 918.

(60) Gayathri, B. R.; Mannekutla, J. R.; Inamdar, S. R. *J. Mol. Struct.* **2008**, *889*, 383.

(61) Shirota, H.; Castner, E. W., Jr. *J. Chem. Phys.* **2000**, *112*, 2367.

(62) Hoyau, S.; Ben Amor, N.; Borini, S.; Evangelisti, S.; Maynau, D. *Chem. Phys. Lett.* **2008**, *451*, 141.

(63) Kaminski, J. W.; Gusarov, S.; Wesolowski, T. A.; Kovalenko, A. *J. Phys. Chem. A* **2010**, *114*, 6082.

(64) Caricato, M.; Mennucci, B.; Scalmani, G.; Trucks, G. W.; Frisch, M. J. *J. Chem. Phys.* **2010**, *132*, 084102.

(65) Aidas, K.; Mikkelsen, K. V.; Mennucci, B.; Kongsted, J. *Int. J. Quantum Chem.*, in press (DOI: 10.1002/qua.22624).

(66) Mata, R. A. *Mol. Phys.* **2010**, *108*, 381.

(67) Sneskov, K.; Matito, E.; Kongsted, J.; Christiansen, O. *J. Chem. Theory Comput.* **2010**, *6*, 839.

(68) Epifanovsky, E.; Kowalski, K.; Fan, P.-D.; Valiev, M.; Matsika, S.; Krylov, A. I. *J. Phys. Chem. A* **2008**, *112*, 9983.

(69) Sulpizi, M.; Röhrig, U. F.; Hutter, J.; Rothlisberger, U. *Int. J. Quantum Chem.* **2005**, *101*, 671.

CT1003803